

The role of $^3\Pi_{0+}$ in the photodissociation of BrCl at 235 nm

Moon-Soo Park, Young-Jae Jung, Sung-Hae Lee, Dong-Chan Kim,
Kyung-Hoon Jung*

*Department of Chemistry and School of Molecular Science (BK21), Korea Advanced Institute of Science and Technology,
Taeduck Science Town, Taejon 305-701, South Korea*

Received 3 September 1999; in final form 10 April 2000

Abstract

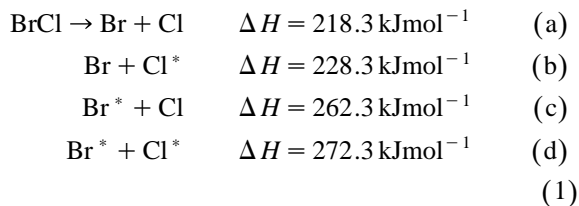
The photodissociation of BrCl has been investigated at 235 nm using a two-dimensional photofragment ion imaging technique. Three direct dissociation channels were observed with the quantum yields of $\Phi[\text{Br}(^2P_{1/2}) + \text{Cl}(^2P_{3/2})] = 0.58 \pm 0.05$, $\Phi[\text{Br}(^2P_{3/2}) + \text{Cl}(^2P_{1/2})] = 0.16 \pm 0.05$, and $\Phi[\text{Br}(^2P_{3/2}) + \text{Cl}(^2P_{3/2})] = 0.26 \pm 0.05$, and angular distributions were represented by anisotropy parameters, $\beta = 1.98 \pm 0.05$, -1.04 ± 0.05 , and 1.88 ± 0.05 , respectively. The results indicate that the $2341\ ^3\Pi_{0+}$ state plays a key role in the dissociation dynamics after absorbing a photon. Based on the results of BrCl and newly found probe lines for Br atoms, the ionization probability ratios of $\text{Cl}(^2P_{3/2}$ or $^2P_{1/2})$ to $\text{Br}(^2P_{3/2}$ or $^2P_{1/2})$ were determined. © 2000 Elsevier Science B.V. All rights reserved.

1. Introduction

The photodissociation dynamics of homo- and heterodiatomic halogens have long been investigated due to their interesting properties such as the avoided crossing and the predissociation of the potential curves [1]. BrCl dissociates into bromine and chlorine which have impacts on ozone depletion [2–4]. BrCl, in addition, can be used as a good reference compound to determine the formation ratio of bromine and chlorine in the dissociation of both bromine and chlorine containing molecules by correlating the exact quantum yield of each dissociation channel of BrCl with their dynamic behaviors.

The halogen atom photofragments are generally formed in two low-lying fine structural states, i.e. the

ground state $\text{Br}(4p\ ^2P_{3/2})$ (denoted Br) and $\text{Cl}(3p\ ^2P_{3/2})$ (denoted Cl), and the first spin-orbit (SO) excited state $\text{Br}(4p\ ^2P_{1/2})$ (denoted Br*) and $\text{Cl}(3p\ ^2P_{1/2})$ (denoted Cl*). In the BrCl photolysis, four one-photon dissociation channels are thermodynamically possible in the ultraviolet (UV) wavelength region.



The bond dissociation energy, $D_0(\text{Br-Cl})$, was determined to be $218.3 \text{ kJ mol}^{-1}$ [5]. The SO excitation energies of bromine and chlorine are 44 and 10 kJ mol^{-1} , respectively [6]. BrCl exhibits a continuous absorption spectrum with three peaks at 225,

* Corresponding author. Fax: +82-42-869-8123; e-mail: khjung@mail.kaist.ac.kr

373, and 443 nm in the UV–visible region [7,8]. The maxima at 373 and 443 nm have been assigned to the transitions from the ground state $X^1\Sigma_0^+$ to the $C^1\Pi_1$ and $B^3\Pi_{0^+}$ states, respectively, arising from the electron configuration $\sigma_g^2\pi_u^4\pi_g^3\sigma_u^1$ (2431) correlated with the dissociation channels as displayed in Fig. 1. A, B and ion-pair states have been studied by laser induced fluorescence (LIF) and emission spectroscopy [9–13]. The nonadiabatic dissociation and predissociation on the B state were investigated [5,14]. The absorption at 225 nm was attributed to $D(0^+) \leftarrow X^1\Sigma_0^+$. The photodissociation dynamics of BrCl in the UV region have been studied via the ion-image technique coupled with the resonance enhanced multiphoton ionization (REMPI) at 235 and 260 nm [15]. In this previous study, however, the photodissociation in the range of 235–540 nm, only two channels ($Br + Cl^*$ and $Br^* + Cl$) could be observed at 235 nm due to the experimental limitation.

Although the electronic states of BrCl corresponding to the transitions in the UV region is not well

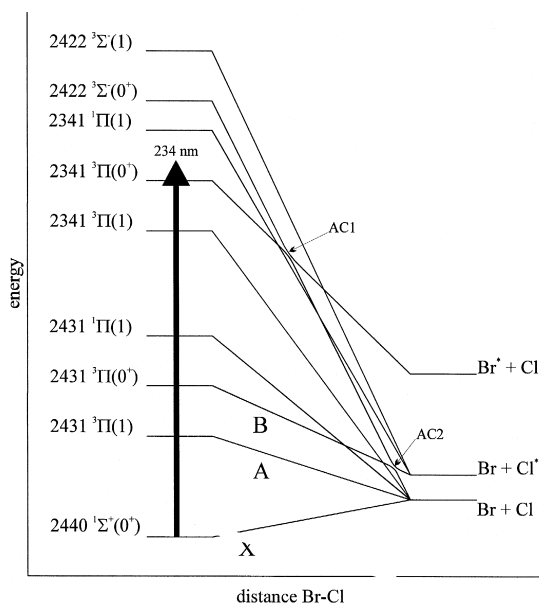


Fig. 1. Adiabatic correlation diagram of BrCl. The transitions which are allowed only to the states with $\Omega = 0$ and 1 are displayed. The vertical arrows represent the excitations by the 235 nm photons.

known, it can be deduced from the well-established properties of other heterodiatomic halogen molecules, ICl and IBr [1,16]. Since ICl has been studied in detail by various spectroscopic and theoretical methods [17–20], its dissociation dynamics can help to understand the electronic structure of BrCl. On the contrary, there are some disagreements among the reported results of ICl at 235 nm. The first disagreement is in the existence of the $I + Cl$ channel. In the REMPI–Doppler profile experiments, three dissociation channels ($I + Cl$, $I + Cl^*$, and $I^* + Cl$) were observed [18], while only two channels ($I + Cl^*$ and $I^* + Cl$) were confirmed in the REMPI–TOF (time of flight) and the ion-image experiments [19]. The second is related to the analysis of the contribution of the $2341^3\Pi_{0^+}$ state. The UV absorption of ICl corresponds to transitions to the $2422^3\Sigma_0^-$, $2341^1\Pi_1$ and $3\Pi_{0^+}$ states from the ground state $X^1\Sigma_0^+$. The $2341^3\Pi_{0^+}$ state adiabatically correlates to the $I + Cl^*$ dissociation channel with avoided crossing 1 (AC1) between the $2422^3\Sigma_0^-$ and the $2341^3\Pi_{0^+}$ state, and avoided crossing 2 (AC2) between the $2341^3\Pi_{0^+}$ and the $2431^3\Pi_{0^+}$ state as shown in Fig. 1, the correlation diagram of BrCl, which is similar to that of ICl. In the REMPI–Doppler study, it has been suggested that the fraction of the $2341^3\Pi_{0^+}$ state is 0.43. Meanwhile a small contribution of this state to the absorption at 235 nm has been assumed with no evidence of any parallel component of the $I + Cl^*$ channel where the parallel component results from the $\Omega = 0^+$ state and the perpendicular component from the $\Omega = 1$ state. In order to evaluate the dissident results, it is very important to determine the exact relative quantum yields for the dissociation channels, (a)–(c) and the nonadiabatic crossing probability at AC2.

In the case of the dissociation of BrCl, two $\Omega = 0^+$ states (the $2422^3\Sigma_0^-$ and the $2341^3\Pi_{0^+}$ states) which strongly contribute to the absorption at 235 nm have been already exhibited as the $Br^* + Cl$ channel. In the present study, we have suggested that two $\Omega = 0^+$ states correlate with the $Br + Cl^*$ and/or the $Br + Cl$ channel irrespective of the nonadiabatic transition at AC1 and AC2. We show the exact dynamics of the $2341^3\Pi_{0^+}$ state of BrCl to verify our suggestion at 235 nm and the possibility of BrCl as a reference compound for the determination of the REMPI strengths for both bromine and

chlorine atoms. We have estimated the ionization probabilities of Br, Br*, Cl, and Cl* near 235 nm. In order to obtain the angular and speed distributions and to determine the branching ratio of each dissociation channel, the fragment ion-image technique was employed. We report REMPI probe lines for bromine atoms in the region of 232–236 nm. We have assigned the low and intermediate states of the 13 two-photon REMPI lines by investigating two-dimensional images and compared them with known literature values [21]. Among these lines, a pair of REMPI probe lines at 233.69 nm for Br and 234.03 nm for Br* were chosen to be good probe lines because the wavelengths are close and the ionization signal intensities are strong.

2. Experiment

The photofragment ion-image system used in this study has been described elsewhere in detail [22]. BrCl (20 Torr seeded in ca. 1.4 atm He) was injected into the reaction zone through a skimmer and a 1 mm pinhole using a pulsed molecular beam valve (General Valve Series 9) operated at 10 Hz. BrCl was synthesized by mixing 200 Torr Cl₂ gas (MG IND. purity > 99.9%) with 10 Torr Br₂ vapor (Aldrich, purity > 99.5%) in a mixing chamber and was kept overnight to reach equilibrium. Because the absorption cross-section of Cl₂ is smaller than those of Br₂ and BrCl at 235 nm (Cl₂: 0.04×10^{-20} , Br₂: 0.9×10^{-20} , and BrCl: 6×10^{-20} cm²), excess Cl₂ in the equilibrium gas (Br₂ + Cl₂ ⇌ 2BrCl: $K_{\text{eq}} = 6.4$) does not interfere with the detection of photofragments from the dissociation of BrCl [8]. CCl₃Br (10 Torr/1.4 atm He) and CF₃Br (20 Torr/1.4 atm He) were injected into the reaction zone in the same manner as BrCl.

A linearly polarized UV laser light (typically 50 μJ/pulse), generated through doubling the output of a Nd:YAG (355 nm) pumped dye laser, was focused perpendicularly onto the ionization zone of the molecular beam with a lens ($f_l = 150$ mm) and paralleled onto an image plane. CCl₃Br, CF₃Br, and BrCl were photolyzed by the UV laser light, and the fragments were then selectively ionized at 235.20 nm for Cl*, at 235.34 nm for Cl, at 234.03 nm for Br*,

and at 233.69 for Br using the [2 + 1]-REMPI technique within the same laser pulse. The laser wavelength was scanned over the range of ca. 4 cm⁻¹ to detect all velocity components of the fragments.

The ion fragment cloud was projected onto a two-dimensional position sensitive detector plate, consists of a microchannel plate (MCP)/phosphor screen (Galileo, FM2040) and a charge coupled device (CCD) camera (Photometric, CH250). The image was summed over at least 10 000 shots and the background was removed by subtracting the reference image collected at an off-resonant wavelength under the same conditions. The TOF mass spectra were acquired using a photomultiplier tube (Hamamatu, 1P21) instead of the CCD camera. The [2 + 1]-REMPI spectrum of bromine atom was obtained by placing a photomultiplier tube at the back of phosphor screen and was scanned between 232 and 236 nm. The ion signals from the phosphor screen were monitored using a boxcar integrator. During the scan, the power of the laser was maintained within ±10%.

3. Result and analysis

3.1. Assignment of 13 REMPI lines for bromine atoms in the region of 232–235 nm

CCl₃Br is used as a source of Br and Cl atoms owing to its large absorption cross-section and high product quantum yields at 235 nm [22]. Thirteen REMPI lines of Br were observed in the region of 232–236 nm as shown in Fig. 2. Since the power dependence of REMPI lines was found to be quadratic, the observed REMPI lines seem to be produced by the [2 + 1] photon process. The wavelengths of REMPI lines in Table 1 were calibrated against the well-established REMPI line of Cl at 235.336 nm ($4p^2D_{3/2} \leftarrow 3p^2P_{3/2}$) [23]. The low and intermediate states of 10 lines among the observed lines were assigned, and they coincide with the literature [21]. Five lines originated from the first excited state of bromine (Br*, $4p^2P_{1/2}$), and the other five lines from the ground state (Br, $4p^2P_{3/2}$). However, it is difficult to assign three lines (numbers 2, 11 and 13 in Table 1) because of the large

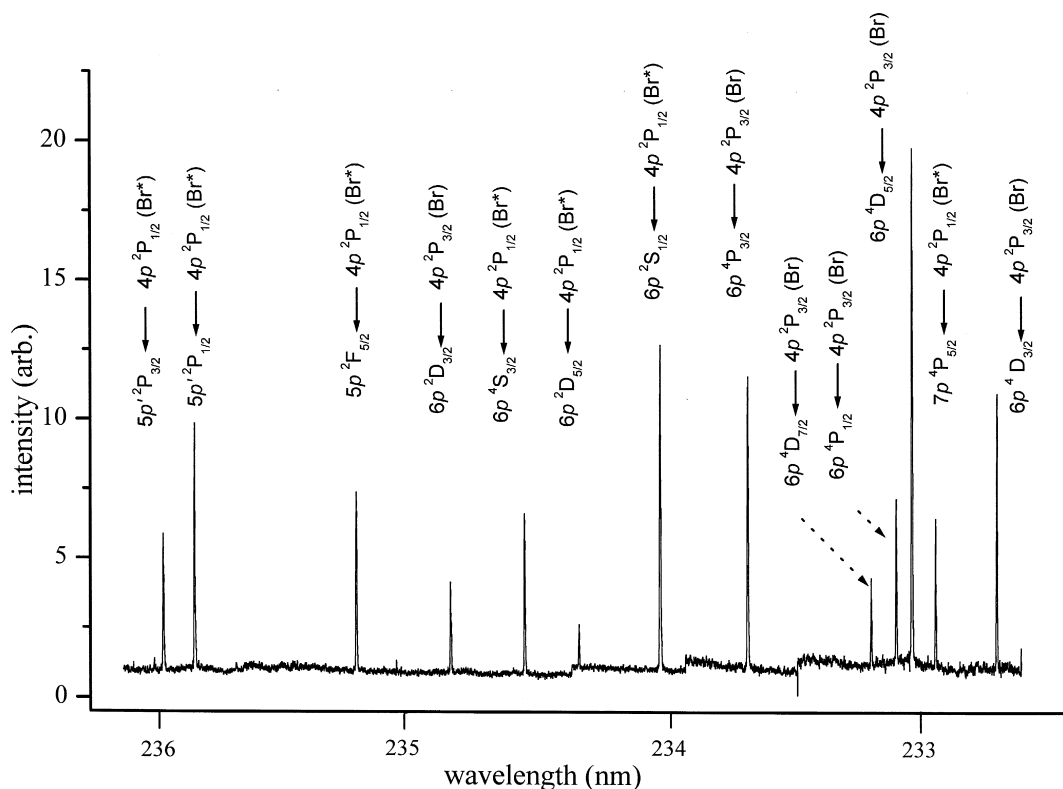


Fig. 2. Two photon atomic transitions of bromine atom: CCl_3Br was used as a precursor.

difference between the obtained values and the reported values. Among these assigned lines, we se-

Table 1

Two photon atomic transitions of bromine in the region of 232–236 nm

No.	Wavelength (nm)	Literature (value) ^b	State	
			Lower ^a	Upper ^b
1	232.72	232.72	Br	$6p^4D_{3/2}$
2	232.96	232.94	Br*	$7p^4P_{5/2}$
3	233.05	233.06	Br	$6p^4D_{5/2}$
4	233.11	233.12	Br	$6p^4P_{1/2}$
5	233.21	233.21	Br	$6p^4D_{7/2}$
6	233.69	233.70	Br	$6p^4P_{3/2}$
7	234.03	234.04	Br*	$6p^2S_{1/2}$
8	234.34	234.35	Br*	$6p^2D_{5/2}$
9	234.56	234.57	Br*	$6p^2S_{3/2}$
10	234.85	234.86	Br*	$6p^2D_{3/2}$
11	235.22	235.32	Br*	$5p^2F_{5/2}$
12	235.86	235.66	Br*	$5p^2P_{1/2}$
13	235.98	235.87	Br*	$5p^2P_{3/2}$

^a Br and Br* refer to the $4p^2P_{3/2}$ and $4p^2P_{1/2}$.

^b Ref. [21].

lected a pair of lines as reference lines, 233.69 nm for Br and 234.03 nm for Br*, to identify the origins of the three lines.

We have investigated the angular distributions of bromine atoms to identify which of the three unassigned lines is from Br or Br*, using the two-dimensional imaging technique. The angular distribution of bromine atoms is given by

$$P(\theta) = \frac{1}{4\pi}(1 + \beta P_2(\cos \theta)) \quad (2)$$

where $P(\theta)$ is the ion intensity at θ angle between the laser polarization axis and the recoil velocity vector, and the β value indicates the anisotropy parameter ($-1 \leq \beta \leq 2$), and $P_2(\cos \theta)$ is the second-order Legendre polynomial. If the β values of Br at 233.69 nm and Br* at 234.03 nm are quite different, we can measure the origins of the unassigned lines by comparing their β values with the β values of reference lines. We have used CF_3Br as a precursor for Br and Br* and observed a large

difference of β values, Br ($\beta = 0.66$) at 233.69 nm and Br* ($\beta = 1.83$) at 234.03 nm [22]. The β values of bromine images acquired at three lines were 1.69 ± 0.10 , 1.65 ± 0.10 , and 1.69 ± 0.10 , respectively. These results show that the three lines originate from Br*. According to the selection rules for the two photon transition of a heavy atom ($\Delta l = 0, \pm 2$, $\Delta J = 0, \pm 1, \pm 2$), the three lines have been assigned in Table 1.

3.2. Photodissociation of BrCl at 235 nm

Since the REMPI technique is highly selective and sensitive, Br and Br* can be ionized selectively at two different resonance wavelengths. The product quantum yields of these two different energy state atoms at a given photolysis wavelength can then be expressed by .

$$\frac{S(\text{Br})}{S(\text{Br}^*)} = \frac{f(\text{Br})_{\lambda_1}}{f(\text{Br}^*)_{\lambda_2}} \frac{N(\text{Br})_{\lambda_1}}{N(\text{Br}^*)_{\lambda_2}} \quad (3)$$

$$= \frac{f(\text{Br})_{\lambda_1}}{f(\text{Br}^*)_{\lambda_2}} \frac{\Phi(\text{Br})_{\lambda_1}}{\Phi(\text{Br}^*)_{\lambda_2}} \frac{\sigma_{\lambda_1}^{\text{R-Br}}}{\sigma_{\lambda_2}^{\text{R-Br}}} \quad (4)$$

$$\approx \frac{f(\text{Br})_{\lambda_1}}{f(\text{Br}^*)_{\lambda_2}} \frac{\Phi(\text{Br})_{\lambda_1}}{\Phi(\text{Br}^*)_{\lambda_2}} \quad (5)$$

where $S(\text{Br})/S(\text{Br}^*)$ is the ion signal ratio of Br and Br*, $f(\text{Br})_{\lambda_1}/f(\text{Br}^*)_{\lambda_2}$ the ionization probability ratio of Br and Br* at their resonance wavelengths, λ_1

and λ_2 . $N(\text{Br})_{\lambda_1}/N(\text{Br}^*)_{\lambda_2}$ denotes the ratio of Br and Br* formed at photolysis wavelengths, λ_1 and λ_2 . $\Phi(\text{Br})_{\lambda_1}/\Phi(\text{Br}^*)_{\lambda_2}$ indicates the ratio of product quantum yields of two different state bromine atoms, and $\sigma_{\lambda_1}^{\text{R-Br}}/\sigma_{\lambda_2}^{\text{R-Br}}$ the absorption cross-sections at two different resonance wavelengths. Using Eq. (4) we can obtain the product quantum yields from the ion signals, when the ionization probabilities of Br and Br* are known.

When these resonance wavelengths of REMPI probe lines, λ_1 and λ_2 , are very close, the absorption cross-sections of alkyl bromide at λ_1 and λ_2 can be approximated to be equal in a practical sense, especially in the case of one-color experiments. Eq. (4) can be approximated by Eq. (5). Further, in order to obtain precise quantum yields, the ionization probabilities of Br at λ_1 and Br* at λ_2 have to be large in order to obtain a high signal-to-noise ratio. The good REMPI probe lines satisfying the conditions of closeness and strong ionization probabilities are useful for determining the branching ratio of X and X*. Among newly found lines, a pair of good REMPI probe lines at 233.69 nm for Br and at 234.03 nm for Br* were chosen.

$f(\text{Br})_{-233.69 \text{ nm}}/f(\text{Br}^*)_{-234.03 \text{ nm}}$ was estimated to be 0.42 ± 0.02 from the Br₂ photolysis under the same experimental condition [24]. In this study, the ratio of $N(\text{Br}^*)/N(\text{Br})$ was found to be 1.38 ± 0.12 . From the ratio, the relative quantum yields, $\Phi(\text{Br}^*)$

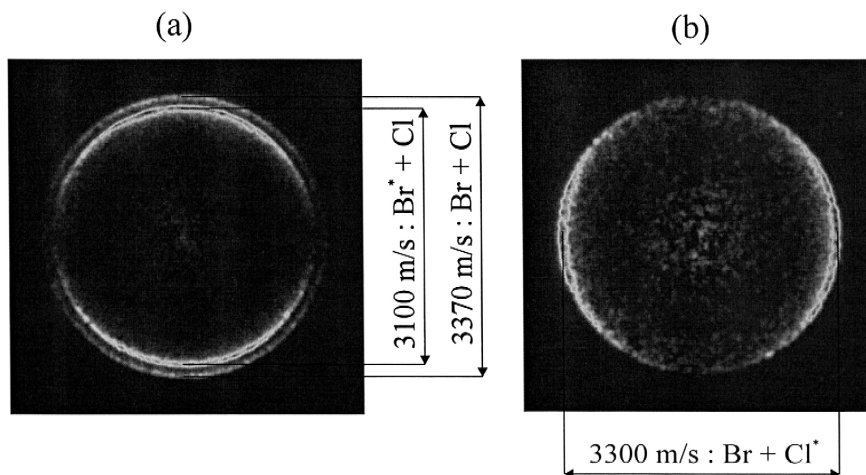


Fig. 3. Raw ion images of the chlorine fragments from the BrCl photolyses at 235 nm. (a) and (b) represent the Cl and Cl* images. The polarization vector of the laser is vertical.

Table 2
The relative quantum yields for three channels

Channel	β	Speed of chlorine fragments	Φ	x_{\parallel}	x_{\perp}
Br* + Cl	1.98 ± 0.05	3101 m s^{-1}	0.58	1	0
Br + Cl*	-1.04 ± 0.05	3306 m s^{-1}	0.16	0	1
Br + Cl	1.88 ± 0.05	3368 m s^{-1}	0.26	0.96	0.04

and $\Phi(\text{Br})$, were determined to be 0.58 ± 0.02 and 0.42 ± 0.02 , respectively. We have measured $N(\text{Br}^*)/N(\text{Br})$ rather than $N(\text{Cl}^*)/N(\text{Cl})$ because $f(\text{Cl})/f(\text{Cl}^*)$ at 235 nm is not available due to the lack of a proper reference compound.

Two-dimensional images of chlorine fragments produced from the BrCl photolysis at 235 nm are displayed in Fig. 3. These raw images are two-dimensional projections of the three-dimensional speed and angular distributions of the chlorine fragments. The Cl image in Fig. 3a shows the characteristics of

the parallel transition while the Cl* image in Fig. 3b shows the characteristics of the perpendicular transition. The projected velocity distributions of the chlorine fragments show maxima at approximately 3370 and at 3100 m s^{-1} as shown in Fig. 3a, and at 3300 m s^{-1} as shown in Fig. 3b. The theoretical recoil speeds of chlorine fragments for the dissociation channels (a)–(c) can be calculated based on the energy and momentum conservation. The internal energy of parent molecule is assumed to be zero under the supersonic molecular beam condition. The

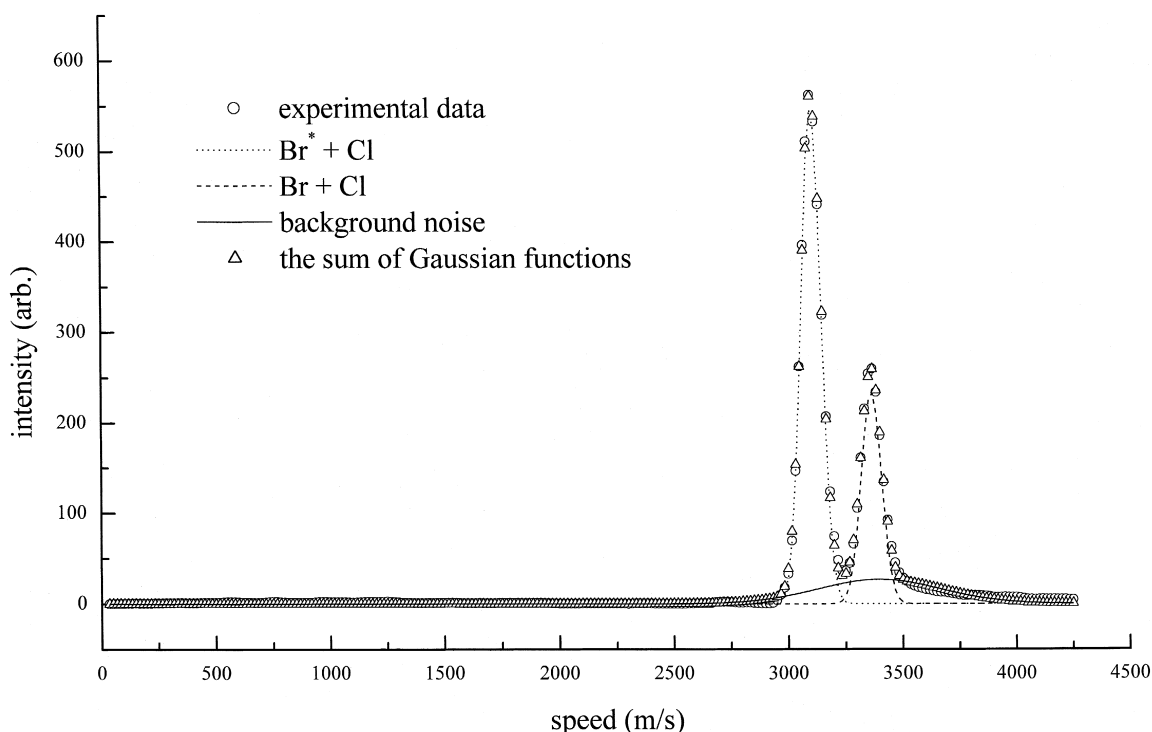


Fig. 4. The speed distribution of Cl fragments at 235 nm (Fig. 3a) is fitted in terms of three Gaussian functions. Two Gaussian functions corresponding to dissociation channels, Br + Cl and Br* + Cl, are displayed in dashed and dot lines, respectively. The straight line indicates another Gaussian function corresponding to background noise. The open triangle denotes the sum of the three Gaussian functions.

calculated speeds for dissociation channels (a)–(c) at 235 nm are listed in Table 2. When the bromine fragments were probed, the translational energy difference between dissociation channels (a) and (b) is only 10 kJ mol⁻¹, which is too small to resolve these channels. Since the translational energy difference between dissociation channels (a) and (c) is 44 kJ mol⁻¹, which is enough to resolve them when the chlorine fragments were probed, the images were acquired to probe chlorine fragments rather than bromine fragments.

In order to reduce the noise effect on the transformation, the raw images were smoothed through the Gaussian filter with a 5 × 5 window and a typical standard deviation of 2 in a pixel unit. Afterwards, they were used to reconstruct three-dimensional velocity distributions by performing the inverse Abel transformation [25,26]. By integrating the reconstructed three dimensional speed distribution over all angles at each speed, the speed distribution for the Cl fragments has been obtained as shown in Fig. 4. The branching ratio, $N(\text{Br}^* + \text{Cl}) / (N(\text{Br} + \text{Cl}) + N(\text{Br}^* + \text{Cl}))$, was obtained from the speed distribution as shown in Fig. 4. Each speed distribution has been fitted into three Gaussian functions, which represent the Br + Cl formation channel, the Br* + Cl channel, and broad background noise. $N(\text{Br}^* + \text{Cl}) / (N(\text{Br} + \text{Cl}) + N(\text{Br}^* + \text{Cl}))$ was calculated by integrating over the fitted functions and found to be 0.69 ± 0.02 as shown in Fig. 4. The relative quantum yield can be calculated from the following relationships and are listed in Table 2.

$$\Phi(\text{Br}^* + \text{Cl}) = \Phi(\text{Br}^*) = 0.58 \pm 0.02 \quad (6)$$

$$\begin{aligned} & \frac{N(\text{Br}^* + \text{Cl})}{N(\text{Br}^* + \text{Cl}) + N(\text{Br} + \text{Cl})} \\ &= \frac{\Phi(\text{Br}^* + \text{Cl})}{\Phi(\text{Br}^* + \text{Cl}) + \Phi(\text{Br} + \text{Cl})} \\ &= 0.69 \pm 0.02 \quad (7) \end{aligned}$$

$$\Phi(\text{Br}^* + \text{Cl}) + \Phi(\text{Br} + \text{Cl}^*) + \Phi(\text{Br} + \text{Cl}) = 1. \quad (8)$$

The angular distribution, $P(\theta)$, has been obtained by integrating the reconstructed three-dimensional speed distribution over a proper range of speed at each angle. θ is the angle between the laser polariza-

tion axis and the recoil velocity of the bromine fragment. The β values extracted from the Cl* and Cl images at 235 nm photolysis are listed in Table 2.

4. Discussion

4.1. The role of $^3\Pi_{0+}$ in the photodissociation of BrCl

In the photolysis of BrCl at 235 nm, three dissociation channels ($\text{Br}^* + \text{Cl}$, $\text{Br} + \text{Cl}^*$, and $\text{Br} + \text{Cl}$) were observed. On the other hand, in the previous study focused in the visible region, only two channels ($\text{Br}^* + \text{Cl}$ and $\text{Br} + \text{Cl}^*$) were observed [15]. A discrepancy similar to that found in the BrCl results was also reported in ICl photodissociation [18,19]. The discrepancy in ICl was attributed to be the misinterpretation of the Doppler spectrum of the Cl fragments, and it was concluded that the $2341 \ ^3\Pi_{0+} \leftarrow X^1\Sigma_0^+$ transition makes a minor contribution to the ICl absorption at 235 nm based on the absence of the I + Cl channel. The Br + Cl channel, therefore, is very important as an evidence of the contribution of the $2341 \ ^3\Pi_{0+}$ state in the photodissociation dynamics in the UV region.

The $2341 \ ^3\Pi_{0+}$ state correlates to the Br + Cl* channel adiabatically via AC1 and AC2 as shown in Fig. 1. Since this channel is also formed from the $2341 \ ^1\Pi_1$ state, it may exhibit both parallel and perpendicular components. In order to estimate the relative contributions of these components to the dissociation channels, classical relationships were used:

$$\beta = x_{\parallel} \beta_{\parallel} + x_{\perp} \beta_{\perp} \quad (9)$$

$$x_{\parallel} + x_{\perp} = 1 \quad (10)$$

β_{\parallel} and β_{\perp} represent the anisotropy parameters for pure parallel and perpendicular transitions. The x_{\parallel} and x_{\perp} values, the fractions for each dissociation channel, are listed in Table 2.

The absorption cross-section corresponding to the transition, $2341 \ ^3\Pi_{0+} \leftarrow X^1\Sigma_0^+$, should be responsible for the parallel component of the Br + Cl* channel and/or the existence of the Br + Cl channel with $\beta = 2$ via nonadiabatic transition at AC2. The anisotropy parameter for the Br + Cl* channel, $\beta =$

-1.04 ± 0.05 , indicates that the $\Omega = 0^+$ state (the $2341\ ^3\Pi_{0^+}$ and/or the $2422\ ^3\Sigma_{0^+}^-$ state) does not contribute to the formation of the Br + Cl* channel. It has been concluded that the channel only arises from the $2341\ ^1\Pi_1$ state. This conclusion coincides with the previous studies of BrCl and ICl systems, in which it is suggested that the contribution of the $2341\ ^3\Pi_{0^+}$ state to the absorption at 235 nm was neglected due to the absence of the parallel component for the Br + Cl* channel [15,18,19]. On the contrary, the discovery of the Br + Cl channel with the quantum yield $\Phi(\text{Br} + \text{Cl}) = 0.26$ in the present study seems not to be in good agreement with the suggestion. The Br + Cl channel can be produced by several pathways as shown in Fig. 1. The pathways with $\Omega = 0$ are (1) the $2422\ ^3\Sigma_{0^+}^-$ state via nonadiabatic transitions at AC1 and at AC2, (2) the $2341\ ^3\Pi_{0^+}$ state via nonadiabatic transition at AC2, and (3) the B $^3\Pi_{0^+}$, while there are (4) the $2341\ ^3\Pi_1$, (5) the $2431\ ^1\Pi_1$, and (6) the A $^3\Pi_1$ states as candidates with $\Omega = 1$. Among these states, (3) B $^3\Pi_{0^+}$, (5) the $2431\ ^1\Pi_1$, and (6) A $^3\Pi_1$ states are excluded since their vertical energies are too low to absorb the photon at 235 nm. According to $\beta = 1.88 \pm 0.05$ for Br + Cl, it can be suggested that the formation of this channel results mainly from the $\Omega = 0^+$ states (the $2422\ ^3\Sigma_{0^+}^-$ and/or the $2341\ ^3\Pi_{0^+}$ state) and the minor portion originates from (4) the $2341\ ^3\Pi_1$ state. However, the exact contribution of the $2341\ ^3\Pi_{0^+}$ state to the formation the Br + Cl channel cannot be measured because the product from the two $\Omega = 0^+$ states (the $2422\ ^3\Sigma_{0^+}^-$ and/or the $2341\ ^3\Pi_{0^+}$ state) were not distinguished in our system. The two results in this study (the strong perpendicular characteristics for Br + Cl* with $\beta = -1.04 \pm 0.05$ and the existence of Br + Cl with $\beta = 1.88 \pm 0.05$) indicate that the $\Omega = 0^+$ state(s) (the $2422\ ^3\Sigma_{0^+}^-$ and/or the 2341

$^3\Pi_{0^+}$ state) does not correlate with the Br + Cl* channel adiabatically but with the Br + Cl channel via nonadiabatic transition at AC2. We suggest that Pr_2 , the nonadiabatic transition probability at AC2, is nearly 1 based on the above statements.

It is possible to determine the range of the contribution of the $2342\ ^3\Pi_{0^+}$ using the relationships with the nonadiabatic transition probability at AC1, Pr_1 :

$$x_{2422\ ^3\Sigma_{0^+}^-} + x_{2341\ ^3\Pi_{0^+}} + x_{2341\ ^1\Pi_1} + x_{2341\ ^3\Pi_1} = 1 \quad (11)$$

$$\Phi(\text{Br}^* + \text{Cl}) = x_{2422\ ^3\Sigma_{0^+}^-}(1 - Pr_1) + x_{2341\ ^3\Pi_{0^+}}Pr_1 \quad (12)$$

where x_i indicates the fraction of the i state. The absorption at 235 nm is assumed to be only due to the transition to the $2422\ ^3\Sigma_{0^+}^-$, the $2341\ ^3\Pi_{0^+}$, the $^1\Pi_1$ and the $^3\Pi_1$ states from the X $^1\Sigma_{0^+}^+$ state. The values of the $x_{2341\ ^1\Pi_1} + x_{2341\ ^3\Pi_1}$ are found to be 0.17 as listed in Table 3. X and Y represent $x_{2422\ ^3\Sigma_{0^+}^-}$ and $x_{2341\ ^3\Pi_{0^+}}$, respectively. Y and Pr_1 can be rearranged into the simple expression:

$$Pr_1 = \frac{Y - 0.25}{2Y - 0.83}, \quad Y = \frac{0.83Pr_1 - 0.25}{2Pr_1 - 1} \quad (13)$$

Two ranges of the contribution of the $2341\ ^3\Pi_{0^+}$ state (Y) and the nonadiabatic transition probability (Pr_1) are calculated from Eq. (13) under the condition of $0 \leq Y \leq 0.83$ and $0 \leq Pr_1 \leq 1$. One set is $0.58 \leq Y \leq 0.83$ and $0.7 \leq Pr_1 \leq 1$. The other is $0 \leq Y \leq 0.25$ and $0 \leq Pr_1 \leq 0.3$. We have excluded the $0 \leq Y \leq 0.25$ and $0 \leq Pr_1 \leq 0.3$ region for two reasons. In the ICl study [19], the high value of the nonadiabatic transition probability (Pr_1) at AC1 has been determined. According to the ICl energy level, the $2422\ ^3\Sigma_{0^+}^-$ state is located at a $4000\ \text{cm}^{-1}$ higher energy than the $2341\ ^3\Pi_{0^+}$ state, which shows a maximum at 235 nm in the Frank–Condon region.

Table 3
The electronic excited states relevant to the channels

Channel	Φ	Assignment
Br* + Cl		0.58
Br + Cl*		0
	\perp	0.16
Br + Cl		0.25
	\perp	0.01

$2422\ ^3\Sigma_{0^+}^-$, $2341\ ^3\Pi_{0^+} \rightarrow 2422\ ^3\Sigma_{0^+}^-$
 $2341\ ^3\Pi_{0^+}$, $2422\ ^3\Sigma_{0^+}^- \rightarrow 2341\ ^3\Pi_{0^+}$
 $2341\ ^1\Pi_1$
 $2341\ ^3\Pi_{0^+} \rightarrow 2431\ ^3\Pi_{0^+}$, $2422\ ^3\Sigma_{0^+}^- \rightarrow 2341\ ^3\Pi_{0^+} \rightarrow 2431\ ^3\Pi_{0^+}$
 $2341\ ^3\Pi_1$

Table 4
Ratios of (2 + 1)-REMPI probabilities of bromine and chlorine atoms

$f(\text{Cl})/f(\text{Br}^*)$	$f(\text{Cl})/f(\text{Br})$	$f(\text{Cl}^*)/f(\text{Br})$	$f(\text{Cl}^*)/f(\text{Br}^*)$
1.24 ± 0.30	3.35 ± 0.84	1.46 ± 0.42	3.94 ± 0.97

* Br, Br*, Cl and Cl* were ionized at 233.69, 234.03, 235.336 and 235.204 nm.

Because of the similarity of ICl and BrCl except for the energy levels of BrCl which are slightly higher than that of ICl, it is expected that the absorption corresponding to the transition to the $2341\ ^3\Pi_{0+}$ state at 235 nm is strong. Consequently, $0.58 \leq x_{2341\ ^3\Pi_{0+}} \leq 0.83$ and $0.7 \leq Pr_1 \leq 1$ have been chosen. The value of 0.58 which resulted from Eq. (6) signifies the lower bound of the contribution of the $2341\ ^3\Pi_{0+}$ state.

In the photodissociation dynamics of BrCl at 235 nm, the quantum yields for the dissociation channels and the angular distribution are reported. The $2341\ ^3\Pi_{0+}$ state has been found to contribute to the formation of the Br + Cl channel. It is suggested that the lower bound of the fraction of the state is 0.58, and the nonadiabatic transition probabilities at AC1 and AC2 with $0.7 \leq Pr_1 \leq 1$ and $Pr_2 = 1$ are obtained.

4.2. Determination of $f(\text{Cl})/f(\text{Br}^*)$

The ion signal intensity, $S(\text{Br})$, is proportional to the ionization probability $f(\text{Br})$ and the sum of the quantum yields of the channels producing Br:

$$S(\text{Br}) \propto f(\text{Br})(\Phi_a + \Phi_b). \quad (14)$$

In order to determine $f(\text{Cl})/f(\text{Br}^*)$, we have measured the ion intensities of Cl and Br* photolyzed from the BrCl precursor and the REMPI probe lines of bromine and chlorine in the region of 233.69–235.34 nm. In TOF mass spectrometry, a long ion flight time decreases the ion peak intensity because of the scattering in the flight region. Controlling the repelling electrode voltage, the flight time of the Cl ion could be adjusted to the same as that of the bromine. The ion peak intensity ratio of Cl and Br*, $S(\text{Cl})/S(\text{Br}^*)$, was 1.80 ± 0.44 . The $f(\text{Cl})/f(\text{Br}^*)$ calculated by Eq. (15) was 1.24 ± 0.30 . Similarly, $f(\text{Cl})/f(\text{Br})$, $f(\text{Cl}^*)/f(\text{Br})$ and $f(\text{Cl}^*)/$

$f(\text{Br}^*)$ were obtained easily using $f(\text{Br})/f(\text{Br}^*)$ and $f(\text{Cl})/f(\text{Cl}^*)$ in Table 4.

$$\frac{f(\text{Cl})}{f(\text{Br}^*)} = \frac{S(\text{Cl})}{S(\text{Br}^*)} \frac{\Phi(\text{Br}^* + \text{Cl})}{\Phi(\text{Br}^* + \text{Cl}) + \Phi(\text{Br} + \text{Cl})}. \quad (15)$$

The newly found good REMPI probe lines are very useful for determining the ratio of quantum yields of Br and Cl producing channels, and thus for investigating the photodissociation reactions of environmentally harmful Br and Cl containing compounds such as polychloro(bromo) dibenzo-*p*-dioxin(PCDD) and CF₂BrCl (halon 1211).

Acknowledgements

The authors gratefully acknowledge the Korea Research Foundation for its support of this research by the Korea–Germany Joint Project, 1998–2001.

References

- [1] M.C. Heaven, Chem. Soc. Rev. 15 (1986) 405.
- [2] L.A. Barrie, J.W. Bottenheim, R.C. Schnell, P.J. Crutzen, R.A. Rasmussen, Nature 334 (1988) 138.
- [3] J.G. Anderson, D.W. Toohey, W.H. Brne, Science 251 (1991) 39.
- [4] E. Tschuikow-Roux, T. Yano, J. Niedzielski, J. Chem. Phys. 82 (1985) 65.
- [5] J. Tellinghuisen, J. Chem. Phys. 89 (1988) 6150.
- [6] C.E. Moore, Atomic Energy Levels, vol. 2 (NSRDS-NBS35 1971).
- [7] D. Maric, J.P. Burrows, G.K. Moortgat, J. Photochem. Photobiol. A: Chem. 83 (1994) 179.
- [8] S. Hubinger, J.B. Nee, J. Photochem. Photobiol. A: Chem. 86 (1995) 1.
- [9] J.J. Wright, W.S. Spates, S.J. Davis, J. Chem. Phys. 66 (1977) 1566.

- [10] J.A. Coxon, *J. Mol. Spectrosc.* 50 (1974) 142.
- [11] M.A.A. Clyne, I.C. Zai, *J. Chem. Soc. Faraday Trans. 2* (1974) 1221.
- [12] A. Hopkirk, D. Shaw, R.J. Donovan, K.P. Lawley, A.J. Yench, *J. Phys. Chem.* 93 (1989) 7338.
- [13] S.W. Brown, C.J. Dowd Jr., J. Tellinghuisen, *J. Mol. Spectrosc.* 132 (1988) 178.
- [14] J. Cao, H.P. Loock, C.X.W. Qian, *Can. J. Chem.* 72 (1994) 758.
- [15] M.J. Cooper, P.J. Jackson, L.J. Rogers, A.J. Orr-Ewing, M.N.R. Ashfold, B.J. Whitaker, *J. Chem. Phys.* 109 (1998) 4367.
- [16] Y.S. Kim, Y.-J. Jung, K.-H. Jung, *J. Chem. Phys.* 107 (1997) 3805.
- [17] C.-K. Ni, G.W. Flynn, *Chem. Phys. Lett.* 210 (1993) 333.
- [18] K. Tonokura, Y. Matsumi, M. Kawasaki, H.L. Kim, S. Yabushita, S. Fujimura, K. Saito, *J. Chem. Phys.* 99 (1993) 3461.
- [19] L.J. Rogers, M.N.R. Ashfold, Y. Matsumi, M. Kawasaki, B. Whitaker, *Chem. Phys. Lett.* 258 (1996) 159.
- [20] K.-W. Jung, T.S. Ahmadi, M.A. El-Sayed, *J. Phys. Chem. A* 101 (1997) 6572.
- [21] C.E. Moore, *Atomic Energy Levels*, vol. 2, NBS Circ. 35, Natl. Bur. Stand., Washington, DC, 1971.
- [22] Y.-J. Jung, M.S. Park, Y.S. Kim, K.-H. Jung, *J. Chem. Phys.* 111 (1999) 4005.
- [23] S. Arepalli, N. Presser, D. Robie, R.J. Gordon, *Chem. Phys. Lett.* 118 (1985) 88.
- [24] Y.-J. Jung, Y.J. Jee, K.-H. Jung, submitted.
- [25] S.M. Candel, *IEEE Trans. Acoust. Speech Signal Proc.* 29 (1981) 963.
- [26] R.N. Zare, D.R. Herschbach, *Proc. IEEE* 51 (1963) 173.